Highly excited vibrational states of HCP and their analysis in terms of periodic orbits: The genesis of saddle-node states and their spectroscopic signature

Christian Beck, Hans-Martin Keller, S. Yu. Grebenshchikov, and Reinhard Schinke
Max-Planck-Institut für Strömungsforschung, D-37073 Göttingen, Germany

Stavros C. Farantos
Institute of Electronic Structure and Laser Foundation for Research and Technology—Hellas, Greece, and Department of Chemistry, University of Crete, Iraklion 711 10, Crete, Greece

Koichi Yamashita
Department of Applied Chemistry, Graduate School of Engineering, University of Tokyo, 7-3-1 Hongo, Tokyo 113, Japan

Keiji Morokuma
Cherry L. Emerson Center for Scientific Computation and Department of Chemistry, Emory University, Atlanta, Georgia 30322

(Received 12 June 1997; accepted 4 September 1997)

We present quantum mechanical bound-state calculations for HCP($\tilde{X}$) using an *ab initio* potential energy surface. The wave functions of the first 700 states, corresponding to energies roughly 23 000 cm^{-1} above the ground vibrational state, are visually inspected and it is found that the majority can be uniquely assigned by three quantum numbers. The energy spectrum is governed, from the lowest excited states up to very high states, by a pronounced Fermi resonance between the CP stretching and the HCP bending mode leading to a clear polyad structure. At an energy of about 15 000 cm^{-1} above the origin, the states at the lower end of the polyads rather suddenly change their bending character. While all states below this critical energy avoid the isomerization pathway, the states with the new behaviour develop nodes along the minimum energy path and show large-amplitude motion with H swinging from the C- to the P-end of the diatomic entity. How this structural change can be understood in terms of periodic classical orbits and saddle-node bifurcations and how this transition evolves with increasing energy is the focal point of this article. The two different types of bending motion are clearly reflected by the rotational constants. The relationship of our results with recent spectroscopic experiments is discussed. © *1997 American Institute of Physics.* [S0021-9606(97)01546-8]

I. INTRODUCTION

Spectroscopy is an extremely powerful tool for determining the structure of molecules.[1] Usually one starts at low excitation energies, deep inside the potential well, and develops a simple Hamiltonian which is able to reproduce the measured spectrum. With increasing energy it becomes necessary to gradually extend the Hamiltonian model in order to take into account higher order effects such as anharmonicities or couplings between the different modes. However, although this rather general approach has been applied very successfully in the past, it is uncertain how far it can be extended. If the energy approaches the dissociation threshold, the mixing between states normally becomes so strong that simple models are bound to fail. Likewise, if the energy comes close to an isomerization barrier, some new dynamical behaviors are expected to develop, which may be difficult to be described by extending pictures appropriate at much lower energies. Thus, either some new models have to be formulated or, alternatively, the problem has to be approached from a different perspective, that is, the exact solution of the Schrödinger equation using a global potential energy surface (PES).

Significant advances have been made in the last years, at least for small molecules, in generating accurate PESs and in solving the multidimensional Schrödinger equation using these surfaces.[2,3] A recent and prominent example is HCO.[4–6] Nonetheless, when one considers highly excited molecules, the density of states is large and consequently hundreds or even thousands of eigenfunctions have to be calculated, which is still a formidable task. Moreover, even if we are able to accurately compute a dense spectrum of vibrational levels, something which becomes more and more feasible with modern computers, the inspection of all these wave functions and their assignment to sets of quantum numbers as well as the extraction of dynamics information from the spectrum are still big challenges.

Because of the problems related to the ''understanding'' of spectra—with ''understanding'' we mean not just the assignment to quantum numbers, which anyhow becomes more and more questionable with increasing energy, but primarily the distillation of dynamical information encoded in the spectra—in the last years tremendous efforts have been made to develop techniques for recognizing patterns and hierarchical coupling in highly congested and complex spectra. We can broadly divide these techniques into statistical and dy-

namical. In the first category we classify methods which employ a special kind of sorting the spectral lines for pattern recognition. Among these techniques we mention the hierarchical tree method of Davis[7,8] and the extended crosscorrelation function method of Field and co-workers.[9] The second category incorporates all semiclassical methods which try to establish a correspondence between quantum states and some classical objects.[10] Once, such a correspondence has been achieved the extraction of dynamics is facilitated through visualization of the nuclear motions offered by classical mechanics.

The validity of semiclassical correspondence is still an open problem, especially at high energies where the classical dynamics turns to be predominantly chaotic. However, after the pioneering works of Gutzwiller[11–13] and Heller[14,15] numerous numerical applications have demonstrated the importance of classical mechanics and especially of periodic orbits (PO) in understanding the localization of wave functions in configuration space, which in turn is helpful for understanding spectral patterns.[16–19]

The concept of POs for tracing the dynamical and spectroscopic characteristics of a polyatomic molecule becomes particularly powerful when it is applied in conjunction with continuation techniques in order to compute families of POs and their energy dependence.[20] This then leads to the construction of continuation/bifurcation diagrams, which are exceedingly helpful for recognizing how spectra change from the bottom of the potential well to highly excited states. The usefulness of POs has been demonstrated for a number of triatomic molecules,[19] and recently even for acetylene, a prototype tetratomic molecule.[21] A few interesting phenomena have been discovered such as the importance of saddle-node states[22] and their connection to the isomerization processes as well as the phenomenon of complex instability.[23] A molecule, for which the understanding of its energy spectrum—on the basis of only the bare quantum mechanical calculations—would be difficult without POs and their continuation/bifurcation diagrams, is HCP in its ground electronic state. In this article we demonstrate how these classical tools can be used to elucidate the patterns in the quantum mechanical spectrum of HCP calculated with an *ab initio* PES.

Recently, the dispersed fluorescence and stimulated emission pumping spectroscopy of phosphaethyne, HCP, performed by Ishikawa *et al.*[24] have raised attention. HCP is similar to HCN. Both of these molecules have linear equilibrium geometries, but they differ in the stability of their linear isomers. While CN–H is a stable isomer, CP–H corresponds to a saddle point on the potential energy surface. The latter has been confirmed by a number of *ab initio* calculations at several levels. Lehmann and co-workers[25] carried out MP4 type calculations for the bending potential and showed that CP–H is a maximum and the same result has been obtained by us with CASSCF/MRSDCI calculations (Sec. II).

Electronic, vibrational, and rotational spectra of HCP have helped to determine the equilibrium geometries and spectroscopic constants of the ground and the first excited electronic states.[25–29] In order to find signatures of large-amplitude angular motion, i.e., isomerization, Field and coworkers have exploited the $\tilde{A}-\tilde{X}$ and $\tilde{C}-\tilde{X}$ transition bands in an attempt to access high lying bending vibrational states.[24] The former band is believed to follow the pure bending overtones $(0,v_2,0)$, with v_2 ranging from 26 to 42, which span an energy interval of $\sim$3 eV above the vibrational ground state. This energy regime is expected to be sufficiently high to allow large-amplitude motion of the H atom around CP.

By fitting the spectra to well known spectroscopic models for linear molecules it was established, however, that despite the energetic opening of a whole new portion of the coordinate space the spectrum is surprisingly regular, as was also found by Lehmann *et al.*[25] some time ago. Nevertheless, two quite surprising observations were made which indicate that indeed a structural change from mainly H–CP to CP–H motion may be entangled. First, with $v_2 \geqslant 32$ perturbations of the pure bending overtones set in which were absent at lower excitations. Second, the vibrational fine structure constants of the $(0,v_2,0)$ levels change abruptly around $v_2=36$. For example, the rotational constant B_0 rises suddenly by about 8% from $v_2=34$ to $v_2=42$. One possible explanation for such a relatively large increase is a substantial change of the molecular structure. The authors conjectured, on the basis of our *ab initio* PES, that the change in the character of H–CP stretch from dominantly H–C to P–H motion should cause a large change in the vibrational level structure and therefore could lead to the sudden turning on of perturbations as well as the abrupt changes in the fine structure constants.[24]

In order to shed some light on these rather surprising findings we have carried out three-dimensional quantum mechanical bound-state calculations employing an *ab initio* PES. In a recent communication (which will be referenced as paper I in what follows) we have presented some preliminary results from our classical and quantum mechanical calculations.[30] The main result was the finding of two distinct families of bending states; one with wave functions confined to small bending angles and the other one sampling the isomerization path all the way from H–CP to CP–H. The former start at low energies and persist to very high energies well above the isomerization plateau, whilst the latter occur abruptly at high energies. Stable periodic orbits provided a clear-cut assignment. The different types of bending motion lead to distinctly different moments of inertia and therefore to different rotational constants. Even though the accuracy of the PES is not good enough to allow direct comparison with the experimental data, it is safe to conjecture that the experimental observations bear some relationship with our predictions of different types of bending motion.

Inspired by our results, Ishikawa *et al.*[31] have performed new SEP experiments in the energy region of $13\,400-17\,500\ \mathrm{cm}^{-1}$ and indeed found strong evidence for the existence of two distinct families of bending states, which they attributed to normal-mode and isomerization-type states, as predicted by the periodic orbit analysis. These new experiments, in turn, encourage us to continue our the-

oretical analysis of the HCP vibrational spectrum at high energies.

In this article we present in detail the classical and quantum mechanical calculations for total angular momentum $J=0$. The main emphasis lies on the development of the spectrum from low energies, where the dynamics is simple and regular, to energies where large-amplitude bending motion is possible and where the spectrum gradually becomes more irregular. In I only the overtones of the various progressions were highlighted; in the present article we discuss all wave functions and analyze their structural changes with increasing energy.

The paper is organized as follows: in Sec. II we present the potential energy surface used in these calculations, and Sec. III features the periodic orbits and their continuation/bifurcation diagrams. In Sec. IV the quantum mechanical results are presented in detail followed by a discussion of the influence of the different bending motions on the rotational constants in Sec. V. In Sec. VI we discuss the relationship of the theoretical predictions to the experimental observations and a summary of the main results ends this article in Sec. VII.

II. *AB INITIO* POTENTIAL ENERGY SURFACE

The HCP ground-state potential energy surface (PES) has been calculated by *ab initio* methods on the multireference configuration interaction (MRCI) level using all singly and doubly excited reference wave functions obtained by complete active space self-consistent field (CASSCF) calculations. A triple-zeta-polarization atomic basis set is employed. For the CASSCF calculations we have chosen 6 electrons and 7 orbitals as the active space giving rise to 142 and 260 reference configuration state functions for linear and bent nuclear geometries, respectively. The MRCI calculations then result in ~78 000 and 156 000 configurations for the two symmetry classes. The calculations have been performed with the MOLPRO program package.[32]

We have computed a total of 157 energies for different geometries sampling a large portion of the coordinate space, especially along the isomerization path. The points are subsequently fitted to an analytical expression of the Sorbie–Murrell form,[33]

$$V(R_1,R_2,R_3)=V^{(3)}(R_1,R_2,R_3)+\sum_{i=1}^{3} V_i^{(2)}(R_i). \tag{1}$$

with R_1, R_2, and R_3 being the HC, CP, and HP separations, respectively. The two-body terms are of the form

$$V_i^{(2)}(R_i)=-D_i(1+a_{1,i}\rho_i+a_{2,i}\rho_i^2+a_{3,i}\rho_i^3)\times\exp(-a_{1,i}\rho_i), \tag{2}$$

where $\rho_i=R_i-R_i^{(e)}$ and the $R_i^{(e)}$ are the equilibrium bond lengths of the three diatoms. The three-body term is written as

TABLE I. Parameters of diatomic potentials.

	a_1/Å^{-1}	a_2/Å^{-2}	a_3/Å^{-3}	D_e/eV	R_e/Å
CH($\tilde{a}\,^4\Sigma^-$)	5.5297	8.7166	5.3082	2.8521	1.0823
CP($\tilde{X}\,^2\Sigma^+$)	4.5794	5.9231	3.6189	5.3568	1.5622
HP($\tilde{X}\,^3\Sigma^-$)	6.2947	12.9232	9.6841	2.0559	1.4029

$$V^{(3)}(R_1,R_2,R_3)=V_0\prod_{i=1}^{3}\left[1-\tanh\left(\frac{\gamma_i\delta_i}{2}\right)\right]\left[\sum_k c_k P_k(s_1,s_2,s_3)\right], \tag{3}$$

where the $P_k(s_1,s_2,s_3)$ are functions in the variables

$$\begin{aligned} s_1&=0.4161\delta_1-0.0975\delta_2+0.9041\delta_3,\\ s_2&=-0.9060\delta_1+0.0400\delta_2+0.4213\delta_3,\\ s_3&=-0.0772\delta_1-0.9944\delta_2-0.0717\delta_3 \end{aligned} \tag{4}$$

(see Table II), and $\delta_i=R_i-R_i^{(0)}$. The two-body parameters $a_{1,i}$, $a_{2,i}$, etc. and the coefficients in Eq. (4) have been taken from Refs. 34 and 35. The coefficients c_k and the reference geometries $R_i^{(0)}$ in the three-body term are fitted to the *ab initio* points. All parameters of the potential function are summarized in Tables I and II.

The subsequent classical and quantum mechanical calculations are performed in Jacobi coordinates R, the distance from H to the center-of-mass of CP, r, the CP separation, and γ, the angle between the vectors **R** and **r** (with $\gamma=0$ for linear HCP; see the inset in Fig. 2). In what follows all energies are quoted with respect to the minimum of H+CP (r_e), i.e., the constant $D_e^{\mathrm{CP}}=5.3568$ eV is added to the full potential. In this normalization the energy at the equilibrium

TABLE II. Parameters of the three-body potential.

$P_k(s_1,s_2,s_3)$	c_k	$P_k(s_1,s_2,s_3)$	c_k
s_1	−0.498 438	s_2	2.033 11
s_3	−2.888 22	s_1^2	−1.124 21
s_1s_2	3.816 18	s_1s_3	−2.218 65
s_2^2	1.085 68	s_2s_3	2.268 83
s_3^2	1.214 87	s_1^3	−0.105 983
$s_1^2s_2$	2.720 32	$s_1^2s_3$	−2.304 62
$s_1s_2^2$	2.159 80	$s_1s_2s_3$	−0.671 877
$s_1s_3^2$	−4.679 40	s_2^3	0.027 829 5
$s_2^2s_3$	0.962 413	$s_2s_3^2$	−3.952 73
s_3^3	−12.732 8	s_1^4	0.090 820 2
$s_1^3s_2$	1.293 98	$s_1^3s_3$	−1.158 38
$s_1^2s_2^2$	1.338 36	$s_1^2s_2s_3$	−0.496 434
$s_1^2s_3^2$	−2.997 57	$s_1s_2^3$	−0.633 082
$s_1s_2^2s_3$	0.566 250	$s_1s_2s_3^2$	−3.253 95
$s_1s_3^3$	−14.803 2	s_2^4	0.088 385 8
$s_2^3s_3$	−0.082 962 5	$s_2^2s_3^2$	0.125 388
$s_2s_3^3$	−2.128 96	s_3^4	−18.082 9
s_2^5	0.098 932 3		
V_0	−0.953 654	γ_1	1.364 91
γ_2	1.437 00	γ_3	1.856 71
$R_1^{(0)}$	2.009 9	$R_2^{(0)}$	1.422 3
$R_3^{(0)}$	2.426 2		

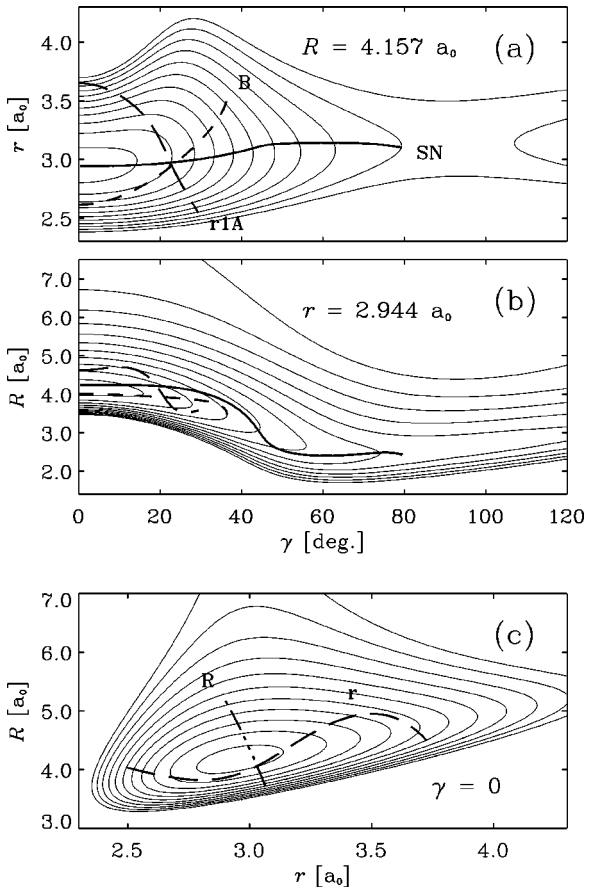

FIG. 1. Contour plots of the HCP potential energy surface as functions of r and γ for fixed value of R (a), R and γ for fixed value of r (b), and R and r for $\gamma=0$ (c). Energy normalization is so that H+CP(r_e) corresponds to $E=0$. The highest contour is for $E=0$ and the spacing is $\Delta E=0.5$ eV. Also shown are the projections of selected classical periodic orbits; (a) and (b) short dashes, $[B]$, $E-2.509$ eV; long dashes, $[r1A]$, $E=-2.500$ eV; solid line, $[\mathrm{SN1}A]$, $E=-2.582$ eV. (c) long dashes, $[r]$, $E=-2.507$ eV; dashed–dotted line, $[R]$, $E=-2.501$ eV.

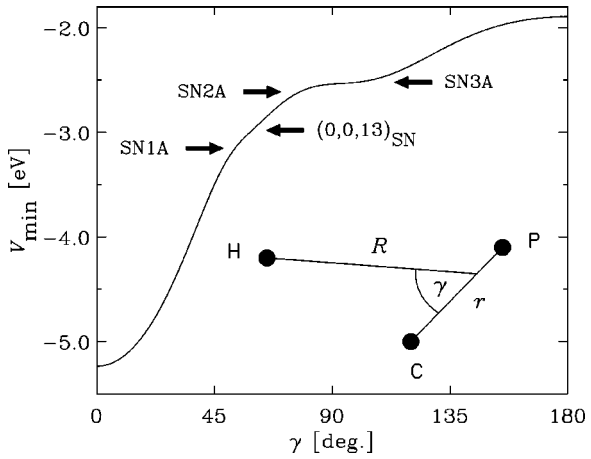

FIG. 2. Potential cut along the minimum energy path as a function of the angle γ. The two stretching coordinates R and r are optimized. Energy normalization is so that H+CP(r_e) corresponds to $E=0$. The four arrows indicate the onset of the periodic orbits of the types $[\mathrm{SN1}A]$, $[\mathrm{SN2}A]$, and $[\mathrm{SN3}A]$ and the position of the first [SN] quantum state (see text). The inset defines the Jacobi coordinates used in the present study.

is -5.2361 eV ($R=4.1572\ a_0$, $r=2.9444\ a_0$, $\gamma=0$). A FORTRAN program of the potential energy surface is available (Ref. 10 in paper I).

Two-dimensional contour plots of the HCP PES are depicted in Fig. 1. Note, that there is no minimum for the CP–H linear configuration but only a saddle point; the upper part of Fig. 1 is misleading, because R is fixed in this representation. The potential contour along the minimum energy path in the angular coordinate is shown in Fig. 2; in order to calculate this energy profile, the potential has been minimized in R and r for a fixed value of γ. The energy and the coordinates of the CP–H saddle point are -1.8935 eV, $R=3.5634\ a_0$, $r=3.0904\ a_0$, and $\gamma=180°$, respectively. For the subsequent discussion it is worth underlining that, as seen in Figs. 1(a) and 1(b) as well as Fig. 2, the behavior of the PES changes quite dramatically in the angular interval between 60° and 90°. This is the region where the bonding changes its character and H–CP begins to more and more go over to CP–H.

Neither the level of the *ab initio* calculations nor the number of calculated points and the analytical fit have been designed to reproduce the true PES near the equilibrium with greatest possible accuracy. Our focus is the vibrational dynamics of highly excited states near the H–CP↔CP–H isomerization. Therefore it does not come as a surprise that the fundamental excitation energies are reproduced only with modest success. The experimental energies for the second overtone of the bending mode, (020), and the first overtones of the CP stretching, (001), and the H–CP stretching, (100), modes are 1332.3 cm^{-1}, 1280.9 cm^{-1}, and 3216.9 cm^{-1}, respectively (Table XI of Ref. 36). The corresponding calculated values are 1283 cm^{-1}, 1234 cm^{-1}, and 3330 cm^{-1}. Two recently published *ab initio* calculations concentrate on the region around the equilibrium and therefore yield much better agreement with these experimental data.[37–39]

III. PERIODIC ORBITS AND PHASE SPACE STRUCTURE

Periodic classical orbits (POs) are located by multiple shooting algorithms and by damped and quasi-Newton iterative methods.[40] According to the Weinstein and Moser theorems[41,42] for a system with N degrees of freedom there are at least N families of periodic orbits, which emanate from the stable equilibrium points of the potential energy surface. These families are called principals and correspond to the N different vibrational modes at energies not too high above the minimum. At a saddle point of a potential one can also find principal families of POs which, however, are unstable in those directions along which the potential descends. By following the evolution of the principal families with total energy, one can locate new families of POs, which bifurcate from the parent ones; they have either the same periods as the original POs or multiples of them. The theory of bifurcations of POs as well as their stability analysis is well developed, and the representation of numerical results is commonly given by a continuation/bifurcation diagram.[43–45]

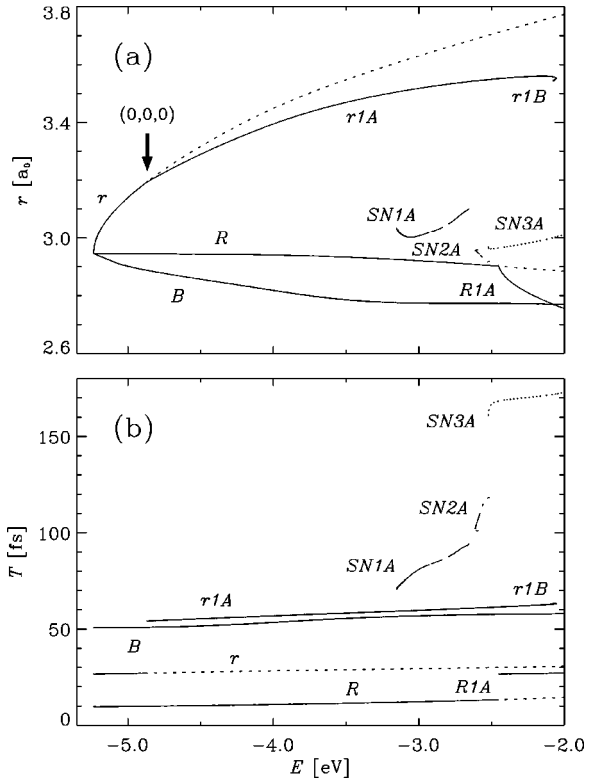

FIG. 3. (a) Continuation/bifurcation diagram. Plotted is the variation of the initial CP stretching coordinate (Ref. 46) as function of energy. The continuous lines represent stable periodic orbits whereas the dots indicate unstable POs. See the text for more details. The arrow indicates the energy of the (0,0,0) ground vibrational state. (b) The periods of the $[B]$-, $[R]$-, $[r]$-, $[r1A]$-, and [SN]-type POs as functions of the energy.

Periodic orbits are either stable or unstable. A periodic orbit is stable when trajectories started close to it stay in its vicinity for all times. On the other hand, a PO is unstable when trajectories, that are launched close to it, depart exponentially, i.e., the ''distance'' between the two trajectories in phase space grows exponentially with time. Whether a periodic orbit is stable or unstable is determined by the eigenvalues of the monodromy matrix, which is calculated by integrating the linearized equations of motion in the vicinity of a PO together with Hamilton's equations.[44,45] If all eigenvalues of the monodromy matrix are pairs of complex conjugate numbers with modulus equal to one, the PO is stable. If one or two pairs of the eigenvalues are real numbers (they come in pairs of λ and $1/\lambda$), the neighboring trajectories deviate exponentially from the PO which is then called singly or doubly unstable, respectively. For systems with three or more degrees of freedom it may also happen that four eigenvalues are related to each other according to λ, $1/\lambda$, λ^*, and $1/\lambda^*$ with modulus different from one; the PO is then called complex unstable.

In Fig. 3(a) we show a projection of the continuation/bifurcation diagram of HCP in the (E,r) plane. The diagram is constructed by plotting the initial value of one particular degree of freedom (the CP bond distance r in the present case) of the POs as a function of the total energy E.[46] If the energy of the system is changed smoothly, then the initial conditions of the PO are also expected to change smoothly, except at bifurcations. The actual shape of the curves in Fig. 3(a) is of course irrelevant; important are only the localizations of bifurcations of families of POs. Continuous lines in the figure represent stable periodic orbits, whereas dots mark unstable ones. We do not distinguish in this diagram the particular type of instability; we note however, that some families do show double and even complex instability, at least for small energy intervals as will be discussed later on. The lower part of Fig. 3 depicts the periods of the periodic orbits vs energy. In Table III we list the period and the initial coordinates and momenta for one representative example out of each family of POs located.[47]

There are three principal families of POs, one for each normal vibrational mode. They will be denoted by $[R]$, $[r]$, and $[B]$, respectively (B stands for bending). Because of the linearity of HCP at the equilibrium point the two stretching periodic orbits, $[r]$ and $[R]$, are constrained to lie in the $\gamma=0$ plane for all times. The $[r]$-type POs represent mainly motion along the CP bond r, whereas $[R]$-type POs show motion mainly along the H–CP stretch coordinate R; examples are depicted in Fig. 1(c). For very low energies, the third principal PO illustrates motion predominantly along the bending angle γ. At higher energies, however, it represents a

TABLE III. Energies E, periods T, and initial conditions for selected periodic orbits.

PO	E/eV	T[a]	R[b]	r	γ	p_R	p_r	p_γ
$[r]$	−2.992 930 4	2.8870	2.396 178 3	1.920 793 4	0.000 000 0	0.449 898 9	−1.103 293 1	0.000 000 0
$[r1A]$	−3.099 328 7	5.8350	2.446 729 7	1.856 564 6	0.106 422 2	0.129 082 9	−1.964 504 7	1.983 991 0
$[R]$	−3.004 148 8	1.1980	2.577 725 5	1.545 207 1	0.000 000 0	1.078 571 3	−1.156 842 9	0.000 000 0
$[R1A]$	−2.290 077 0	2.6269	2.590 402 0	1.492 402 2	0.000 000 0	1.128 202 6	−2.315 557 8	0.000 000 0
$[B]$	−3.069 214 7	5.5700	2.119 118 6	1.467 732 0	0.230 794 2	−0.160 271 6	3.050 687 4	2.867 355 7
$[SN1A]$	−3.026 447 4	7.8251	2.227 777 0	1.589 036 4	−0.304 198 9	−0.543 705 3	0.469 745 8	−3.561 653 0
$[SN1B]$	−3.135 209 1	6.8771	2.281 998 2	1.608 939 2	0.098 053 3	0.031 112 9	0.064 933 0	−4.026 377 6
$[SN2A]$	−2.603 105 6	10.2900	2.243 110 0	1.561 766 8	0.107 014 8	−0.027 608 3	−0.153 367 7	−4.506 792 4
$[SN2B]$	−2.611 706 2	9.9900	2.237 286 2	1.564 291 9	0.124 621 2	−0.061 508 8	−0.142 299 9	−4.484 219 0
$[SN3A]$	−2.122 777 2	16.8320	2.315 583 3	1.584 481 7	0.016 886 4	0.013 950 6	−0.023 606 8	−4.977 894 1
$[SN3B]$	−2.515 965 5	15.4320	2.237 877 2	1.573 123 7	0.100 093 8	−0.078 068 2	−0.056 191 9	−4.599 228 1

[a]One time unit corresponds to 10.18 fs.
[b]Distances in Å, angle in rad, and masses in units of 1/12 of ^{12}C.

mixture of bending and CP stretching motion as will be discussed below.

The family of $[R]$-type POs remains stable up to about 3 eV above the bottom of the well. It becomes singly unstable at -2.454 eV but turns stable again at -1.954 eV. Then, it stays stable up to -0.707 eV where again it becomes singly unstable. However, the real eigenvalue of the monodromy matrix never exceeds the value of 1.2, that is, the POs of type $[R]$ remain reasonably stable for almost the entire energy regime up to the dissociation threshold. A bifurcating family, denoted by $[R1A]$ (branch A of the first bifurcation), comes into existence at -2.454 eV, where the $[R]$-type POs become unstable for the first time. These POs are also confined onto the $\gamma=0$ plane. The period of the new family is roughly twice as large as for the original $[R]$ PO.

The bend family, $[B]$, is also found to be stable up to energies close to dissociation. A prototype is shown in Figs. 1(a) and 1(b) and more examples can be found in Figs. 1 and 2 in paper I. The characteristic feature of these POs is their confinement to relatively small angles; they never explore angles greater than 40°–50° irrespective of the total energy. This behavior seems to be counterintuitive; by pumping more and more energy into the bending mode one expects the bending-type orbit to follow the isomerization path in Fig. 1(b). However, that is not the case. Increasing the energy gradually pushes the orbit towards stretching of the CP mode rather than increasing γ. This rather unexpected behavior is the result of strong mixing between the bending and the CP stretching mode.

Contrary to the other two principal families, the $[r]$ family shows an early bifurcation at -4.872 eV, i.e., only 0.358 eV above the minimum. For comparison, the energy of the ground vibrational state is -4.866 eV, that is, the bifurcation occurs even below the lowest quantum mechanical state. (In the next section we shall show that there are no quantum mechanical states with wave functions following the $[r]$-type PO.) At the bifurcation point a pair of eigenvalues of the monodromy matrix is equal to -1, i.e., this is a bifurcation by reflection, and we denote the bifurcating family as $[r1A]$ (branch A of the first bifurcation). Beyond the point of bifurcation the $[r]$ family becomes singly unstable and remains singly unstable up to $+0.401$ eV. However, the real eigenvalue of the monodromy matrix, which characterizes the degree of the instability of these POs, never exceeds the value of 1.74. The bifurcating POs, $[r1A]$, are stable and remain stable up to -2.056 eV, where they abruptly cease to exist. Actually, from the bifurcation diagram we can see that the $[r1A]$ family originates from a reverse saddle-node bifurcation occurring at the energy of -2.056 eV. Here it merges with a branch of unstable periodic orbits, which is termed $[r1B]$. We found it very difficult to propagate this unstable branch backwards in energy. Numerical difficulties arose because of nearby unstable POs which cause problems in the convergence of the Newton–Raphson procedure, rather than the magnitude of the instability of the $[r1B]$-type POs. In contrast to the $[r]$ POs, the POs of type $[r1A]$ are not confined to the $\gamma=0$ plane but sample regions of coordinate space with nonlinear geometries. Actually, they are symmetric with respect to $\gamma=0$ and therefore their period is roughly twice the period of the $[r]$ POs [see Fig. 3(b)]. An example is shown in Figs. 1(a) and 1(b) (see also Figs. 1 and 2 in paper I). They show a behavior in the (r,γ)-plane, which is opposite to the behaviour of the $[B]$-type POs.

As seen in Table III as well as Fig. 3(b) the periods of the $[B]$ and $[r1A]$ POs are almost identical; the same is obviously true for the quantum mechanical frequencies belonging to the states, which correspond to these POs. It is this accidental coincidence of periods which causes the resonance and polyad structure governing the entire HCP spectrum up to high energies. It is important to underline that the $[r1A]$ POs, like their counterparts of type $[B]$, are confined to small bending angles. In other words, none of the periodic orbits emanating from the bottom of the well samples the isomerization path.

The first POs that extend to angles larger than 40°, i.e., towards the CP–H side of the PES, are found to occur suddenly at an energy of -3.1526 eV or 2.08 eV above the bottom of the well. They emerge from a saddle-node (SN) bifurcation and therefore we denote them as [SN1]. There are again two branches, a stable one, which will be denoted by $[\mathrm{SN1}A]$, and an unstable one, $[\mathrm{SN1}B]$, which we did not follow as function of E. A representative example for branch A is depicted in Figs. 1(a) and 1(b) (see also Figs. 1 and 2 in paper I). The [SN1]-type POs follow closely the minimum energy path in the (R,γ)-plane. However, in contrast to the $[B]$- and $[r1A]$-type periodic orbits they show only little variation in the r coordinate, less than about 0.2 a_0.

The originally stable POs of the $[\mathrm{SN1}A]$ family become singly unstable at -2.927 eV, change into complex unstable at -2.899 eV, and then become again stable at -2.781 eV. Finally, they become once more singly unstable at -2.668 eV and remain singly unstable up to the highest energy we have followed them. The SN1 branch does continue to energies higher than shown in Fig. 3. However, it becomes more and more difficult to find these types of trajectories and therefore we did not systematically follow the SN1 branch any further. At higher energies we have located additional saddle-node bifurcations at -2.612 eV and -2.522 eV, giving rise to new types of periodic orbits. These POs, which are denoted as [SN2] and [SN3], penetrate deeper and deeper into the CP–H hemisphere. The [SN3]-type POs show some oscillatory behaviour in the (R,γ)-plane close to their turning points at larger angles. From Fig. 3(b) it is apparent that, in contrast to the $[B]$- and $[r1A]$-type orbits, the periods of the orbits of the [SN1] and [SN2] families strongly increase with energy. This is readily understandable because the [SN] orbits extend to larger and larger angles where the potential becomes gradually flatter (see Fig. 2).

The overall dynamical behavior of HCP, as it emerges from the continuation/bifurcation diagram, is rather regular, despite the early appearance of a bifurcation and the approximate 1:1 relationship between the vibrational periods of the $[B]$- and the $[r1A]$-type POs. Instability is developed at relatively high energies and only when the bending angle extends well into the CP–H side of the potential. Because the bending family remains stable for the entire energy interval

studied, the unstable regions in phase space are essentially related to the unstable $[r1B]$ family. We will show in the next section that the POs are extremely useful for understanding the quantum mechanical wave functions and their development with energy.

IV. VIBRATIONAL LEVELS AND EIGENFUNCTIONS

A. Variational calculations

We have performed quantum mechanical variational calculations for determining the vibrational energies as well as the corresponding wave functions. The total angular momentum is $J=0$ in all cases. The Hamiltonian is represented in a highly contracted/truncated 3D basis as described in detail in Ref. 48. The variational program requires basically two parameters. The energy E_{cut} up to which all internally contracted basis functions are included and the maximal distance in the dissociation coordinate, R_{max}. All other parameters are chosen automatically. In the present calculations we used $E_{\mathrm{cut}}=-0.2$ eV and $R_{\mathrm{max}}=7.5\ a_0$ resulting in about 9000 basis functions. The estimated error due to limitations of the basis size is less than 1 meV for levels up to 3 eV above the bottom of the well, the energy region most interesting for the present study. Since our PES does not have spectroscopic accuracy, slight errors in the vibrational energies are not considered to be crucial. It is well known that wave functions converge more slowly than energy levels. Nevertheless, we are confident that the main results of this work are not affected by convergence problems as calculations with fewer basis functions have demonstrated.[49,50]

We have visually examined, by both 2D projections and 3D representations, the lowest 700 wave functions in an attempt to assign the vibrational levels. As we will demonstrate, the spectrum is straightforwardly assignable up to an energy of roughly -3 eV, i.e., 2.25 eV above the minimum. Around this energy regime some of the wave functions begin to behave drastically differently, which gradually complicates an unique assignment. Interestingly, this is the same energy regime, in which the saddle-node POs, [SN1], suddenly come into existence. In the following subsections we will describe the assignment of the levels and the relationship between the localization of the quantum wave functions on one hand and the periodic orbits on the other. The effect of the different behaviors of the wave functions on the rotational constants will be elucidated in the next section.

In the subsequent discussion we will use the following notation: ν_1, ν_2, and ν_3 are the H–CP stretch mode associated with R, the bending mode, and the CP stretch mode related to motion in r, respectively. As mentioned in Sec. III, the periods associated with the $[r1A]$- and the $[B]$-type POs are very close, and therefore both types of orbits show a strong mixing of CP-stretching and bending motion. The same resonance effect obviously governs the quantum mechanical dynamics with the consequence that the wave functions are arranged in the (r,γ)-plane rather than along the angular axis or the CP stretching mode. Therefore, the assignment in terms of bending and CP stretching states is quite arbitrary (see below). As will become apparent later on,

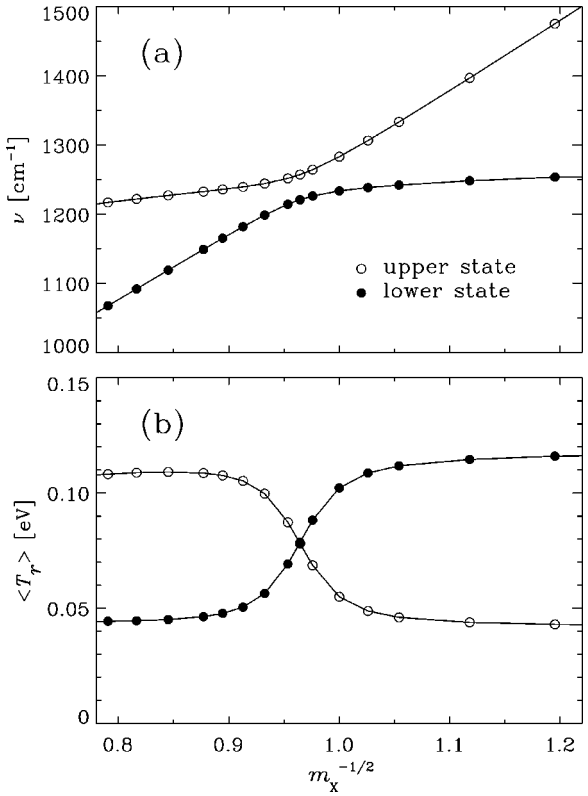

FIG. 4. (a) Variation of the excitation energies of the first two excited states of XCP with $m_{\mathrm{X}}^{-1/2}$. The mass is measured in terms of the hydrogen mass, i.e., $m_{\mathrm{H}}=1$. (b) Variation of the expectation value of the kinetic energy operator associated with the CP stretching coordinate r with $m_{\mathrm{X}}^{-1/2}$.

the wave functions of the two progressions $(0,v_2,0)$ and $(0,0,v_3)$ qualitatively behave in a similar way as far as the symmetry with respect to linearity is concerned. For this reason we prefer an assignment which treats both modes correspondingly and therefore we identify in both cases the quantum numbers v_2 and v_3 with the number of nodes along the ''backbone'' of the respective wave functions in the interval $[0\leqslant\gamma\leqslant\pi]$. This facilitates, as we think, the subsequent discussion. Thus, in order to compare with the usual nomenclature for a linear molecule (including the notation used by us in paper I) the quantum number v_2 has to be multiplied by 2.

B. Polyad structure

The energy spectrum of HCP is governed by a pronounced anharmonic resonance between the bending and the CP stretching modes leading to a distinct polyad structure in the energy level spectrum. This resonance and the corresponding mode mixing is intriguingly illustrated by continuously changing one parameter in the Hamiltonian, for example the mass of the hydrogen atom.[6,51] In Fig. 4(a) we plot the excitation energies [measured with respect to the (0,0,0) ground vibrational state] for the two lowest excited states as a function of $m_{\mathrm{X}}^{-1/2}$ from $m_{\mathrm{X}}\approx 0.7$ to ≈ 1.6 (m_{X} is measured in terms of the mass of the hydrogen atom). The CP stretching frequency is, in a diabatic sense, almost independent of the mass of the attached atom X, whereas the bending frequency varies approximately linearly with $m_{\mathrm{X}}^{-1/2}$. However,

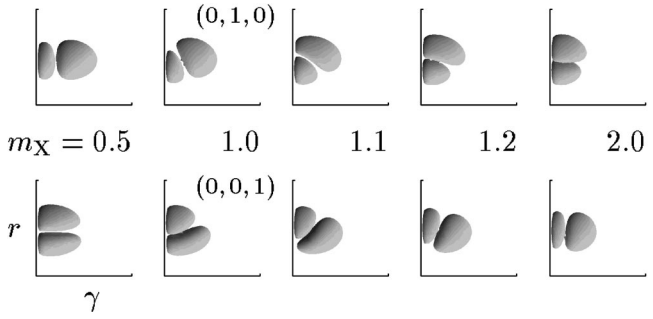

FIG. 5. Wave functions of the first excited (lower panel) and the second excited (upper panel) state for selected values of m_X. The horizontal axis ranges from $\gamma=0$ to 40° and the vertical axis ranges from $r=2.5\ a_0$ to $3.5\ a_0$. For more details see Ref. 52.

according to Wigner's noncrossing rule, the two energy curves are not allowed to cross and therefore are forced to avoid each other. The resulting avoided crossing occurs (accidentally) around $m_X \approx 1.1$, i.e., just in the region of HCP. At small values of m_X the CP stretching (bending) state is the lower (upper) one and the wave function is clearly aligned along the r-(γ-) axis (see Fig. 5 and Ref. 52). As the mass of the atom X increases these two local-mode wave functions mix which results in a rotation in the (r,γ)-plane. At larger values of m_X the wave functions are again aligned along either the one or the other axis and the assignment in terms of local modes is again straightforward.

The effect of mixing is also illustrated by the variation of the expectation values $\langle T_x \rangle$ for the kinetic energies in coordinates $x=r$ or γ. The lower part of Fig. 4 depicts T_r as a function of $m_X^{-1/2}$ for the two states considered. The location of the avoided crossing at $m_X \approx 1.1$ is well predicted by this quantity. In view of this figure it appears that for HCP the upper state has more character of bending motion and therefore should be assigned as (0,1,0), while the lower state has more character of motion along r and thus must be assigned as (0,0,1). This nomenclature is in accordance with the experimental assignment.[36] Incidentally we note that for HCP there is no state with nodes aligned purely along the r axis, which is in accord with the bifurcation into $[r]$- and $[r1A]$-type POs occurring very early, below the vibrational ground state.

The two adiabatic wave functions can be approximately represented by linear combinations of zero-order or local-mode type wave functions according to

$$\Psi_1(r,\gamma) = \cos\eta\ \phi^{(r)}_{k=1}(r)\,\phi^{(r)}_{l=0}(\gamma) - \sin\eta\ \phi^{(r)}_{k=0}(r)\,\phi^{(\gamma)}_{l=2}(\gamma), \tag{5}$$

$$\Psi_2(r,\gamma) = \sin\eta\ \phi^{(r)}_{k=1}(r)\,\phi^{(\gamma)}_{l=0}(\gamma) + \cos\eta\ \phi^{(r)}_{k=0}(r)\,\phi^{(\gamma)}_{l=2}(\gamma),$$

where η is the mixing angle and $\phi^{(r)}_k(r)$ and $\phi^{(\gamma)}_l(\gamma)$ are one-dimensional oscillator wave functions in r and γ with k and l quanta, respectively. The wave functions for HCP are well represented by $\eta \approx \pi/4$.

Because of the resonance in the bending and the CP stretching frequencies, the energy spectrum of HCP consists of well defined polyads $(v_1, P-n, n)$ with polyad quantum

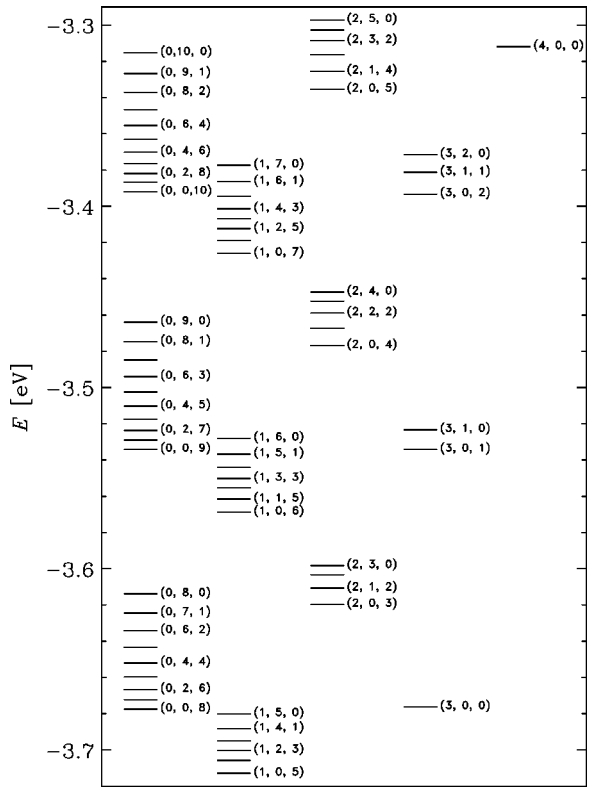

FIG. 6. Section of the energy spectrum in the region of polyads $P=8-10$. The assignment has been made in terms of the nodal structure of the wave functions. All states can be unambiguously assigned.

number $P=v_2+v_3$. Figure 6 shows a portion of the spectrum in the energy region of $P=8-10$. Each polyad, for a fixed value of v_1, consists of $P+1$ levels. The highest one, $(v_1,P,0)$, is the pure overtone of the bending mode, while the lowest member $(v_1,0,P)$ is the overtone of the CP stretching mode associated with r. In order to illustrate the development of the nodal pattern in the low-energy regime we show in Fig. 7 wave functions in polyads $P=1-3$. The relationship of the $(0,P,0)$ and the $(0,0,P)$ wave functions is clearly seen. The potential plot also includes the POs of the $[B]$- and the $[r1A]$-type for the energies of the states (0,3,0) and (0,0,3), respectively. As expected, they follow closely the ''backbone'' of the corresponding wave functions.[19] In full accordance with the classical calculations, both the bending wave functions as well as the CP stretch wave functions are well confined to small angles and this does not change when the energy increases. They do not follow the minimum energy path in the (R,γ)-plane but are more and more pushed aside, to larger respectively smaller values of r. The first wave functions that extend well beyond 40° correspond to the [SN]-type periodic orbits found in the classical analysis. How these states emerge as a function of energy and how they fit into the polyad structure described above is the topic of the next subsection.

Vibrational resonances and polyads are well known topics in molecular spectroscopy (see Refs. 53 and 54, and references therein). We described the polyad structure for HCP

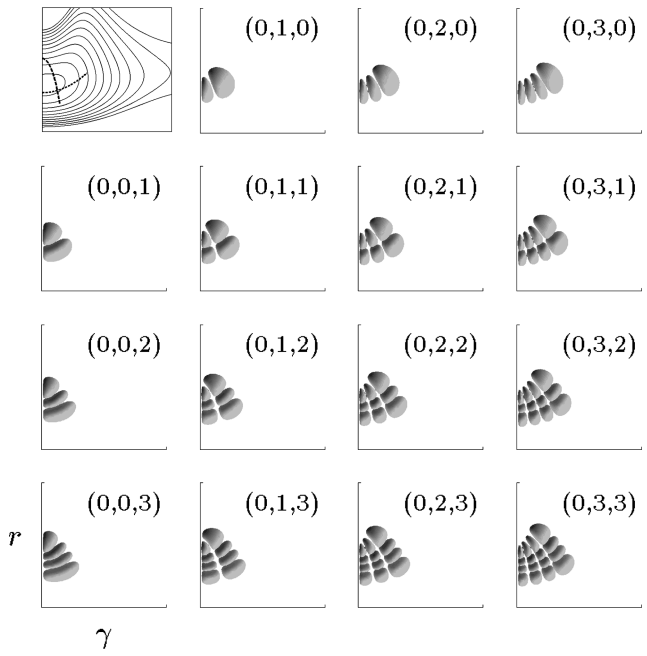

FIG. 7. Wave functions in the low-energy range of the HCP spectrum. The horizontal axis ranges from $\gamma=0$ to 80° and the vertical axis ranges from $r=2.32\ a_0$ to $4.00\ a_0$. For more details see Ref. 52. In order to indicate how the wave functions are arranged in the potential well the panel in the upper-left corner shows a (r,γ) cut of the PES for $R=4.157\ a_0$. Also shown are POs of the $[B]$- and the $[r1A]$-type; the energies of the orbits are those of states (0,3,0) and (0,0,3), respectively.

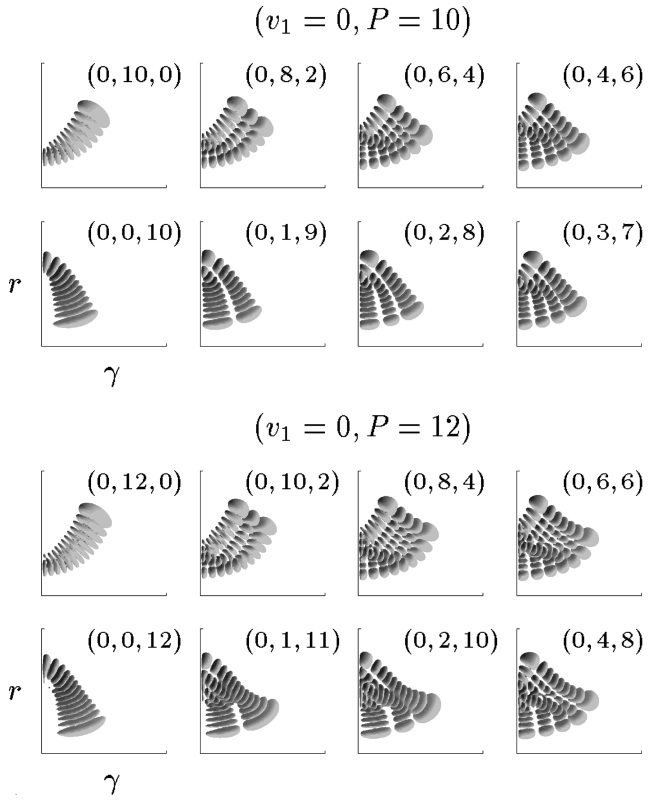

FIG. 8. Selected wave functions in polyads $P=10$ (upper panel) and $P=12$ (lower panel). For more details, see Fig. 7.

in some detail in order to highlight the structural changes that occur at higher energies.

C. The genesis of saddle-node states

All states up to $P=12$ can be—without any real problems—uniquely assigned. In order to illustrate how the wave functions change, within a given polyad, from the lowest to the highest level, we show in the upper panel of Fig. 8 selected wave functions for $P=10$. The transition from (0,10,0), the highest state in this polyad, to (0,0,10), the lowest level, is very ''smooth.'' Coming from the top of the polyad, the number of nodes in the $[r1A]$-type mode gradually increases at the expense of the number of nodes in the $[B]$-type mode. Between states (0,6,4) and (0,4,6) the overall character of the wave function changes from predominantly $[B]$ type to $[r1A]$ type. As we have shown in paper I, the backbone of the wave functions closely follow the $[B]$ and the $[r1A]$ POs (see also Fig. 7). The assignment in terms of two quantum numbers v_2 and v_3 is straightforward; v_1 is zero for all these examples. Polyad $P=11$ behaves in an almost identical manner.

All the wave functions for $P=12$, shown in the lower panel of Fig. 8, are still more or less straightforwardly assignable in terms of nodes along their backbone. However, careful inspection reveals that the nodal pattern of the lower members, e.g., (0,1,11)–(0,4,8), are slightly distorted in comparison to the corresponding $P=10$ wave functions. While all wave functions for $P=10$ are directed either ''up'' (towards larger values of r) or ''down'' (towards smaller values of r), thereby avoiding the isomerization path, the wave functions at the bottom of polyad $P=12$ show some tendency for pointing to larger angles, i.e., in the direction of the CP–H channel. States with a new type of bending wave functions are about to emerge! The lowest member, (0,0,12), however, has again the expected clear structure as all other $(0,0,P)$ wave functions for $P=1-11$.

Something really new begins with $P=13$. This can be seen both in the energy-level structure, Fig. 9, and in the wave functions, Fig. 10. While for $P\leqslant 12$ all polyads are complete, i.e., there are $P+1$ levels, with $P=13$ they begin to become ''incomplete.'' What do we mean by that? At the lower end of this polyad, where the lowest state for $P=13$, (0,0,13), is expected, there is no state which would readily fit into the $(0,P=13)$ scheme. There is a level with a slightly lower energy. However, its wave function does not have the general shape of $(0,0,P)$-type wave functions observed for $P\leqslant 12$ (see Figs. 7 and 8). While the $(0,0,P\leqslant 12)$ wave functions show curvature in the (r,γ)-plane, this wave function runs almost parallel to the r axis, but at the same time clearly extends to larger angles. It is very much reminiscent of the [SN]-type POs discussed above (see Fig. 14 and paper I). This wave function has 13 nodes along its backbone and therefore we include it to the $P=13$ polyad, despite the fact that its energy does not fit to the polyad structure. However, one should keep in mind that this state is somewhat different. In order to distinguish it and other examples from the ''pure'' (v_1,v_2,v_3) states we will use the index SN.[55] The

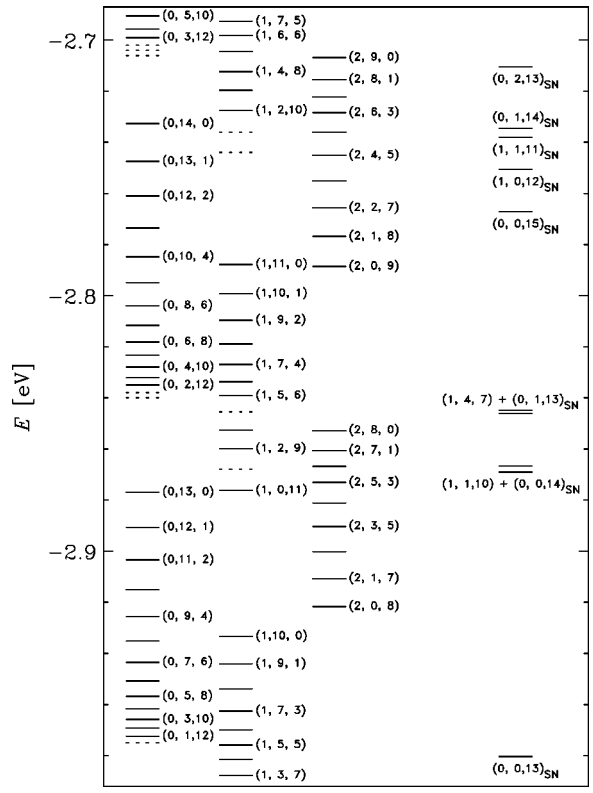

FIG. 9. Section of the energy spectrum in the region of polyads $P=13-15$. The assignment has been made in terms of the nodal structure of the wave functions. Levels, which do not readily belong to the clear polyad structure observed at lower energies, are given in the right-hand column. They are mostly of the [SN] type and therefore labeled by $(v_1,v_2,v_3)_{SN}$. The dotted lines do not represent calculated energy levels, but indicate missing levels.

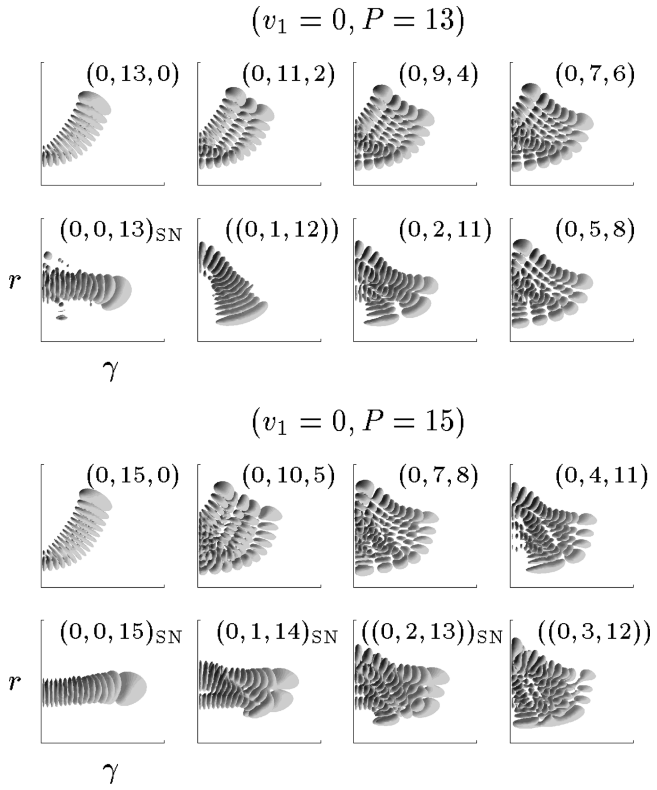

FIG. 10. Selected wave functions in polyads $P=13$ (upper panel) and $P=15$ (lower panel). For more details see Fig. 7.

first clear-cut SN-type state occurs at an energy just slightly higher than the first [SN]-type PO (Fig. 2).

The trend observed for $P=13$ continues to higher polyads and actually becomes even more pronounced. For example, for $P=14$ already two states are missing at the lower end of this polyad, (0,1,13) and (0,0,14). There are two pairs of levels at significantly lower energies, which cannot be clearly assigned (Nos. 246 and 248, respectively, 254 and 255). One level of the lower pair is certainly $(0,0,14)_{SN}$, and one level of the upper pair is state $(0,1,13)_{SN}$. However, due to substantial mixing with states of the $P=11$ polyad with $v_1=1$ the corresponding wave functions have a very bizarre nodal structure.

For $P=15$ three levels are missing at the lower end of the polyad. At the same time two states of the $(1,P=12)$ polyad are absent. Altogether, there are now five states in this energy regime, which do not readily fall into the polyad structure as it is found at lower energies. The wave functions, three of which are plotted in the lower panel of Fig. 10, all have a clear [SN]-type behavior and are assigned to $(0,0,15)_{SN}$, $(0,1,14)_{SN}$, and $(0,2,13)_{SN}$. The remaining two states are assigned to $(1,0,12)_{SN}$ and $(1,1,11)_{SN}$. This kind of evolution continues at higher energies, that is, more and more states at the lower end of a polyad turn into [SN]-type states. However, because the density of states and therefore the mixing between states gradually increases, the assignment becomes more and more tedious and fewer and fewer states can be uniquely assigned.

Close inspection of the wave functions has revealed that starting with polyad $P=13$ the lower states of a polyad gradually change their character from $[r1A]$- to [SN]-type. The onset of this new type of behavior is reflected also by the energy dependence of the various progressions. Figure 11 depicts the energy levels for the two progressions $(0,P,0)$

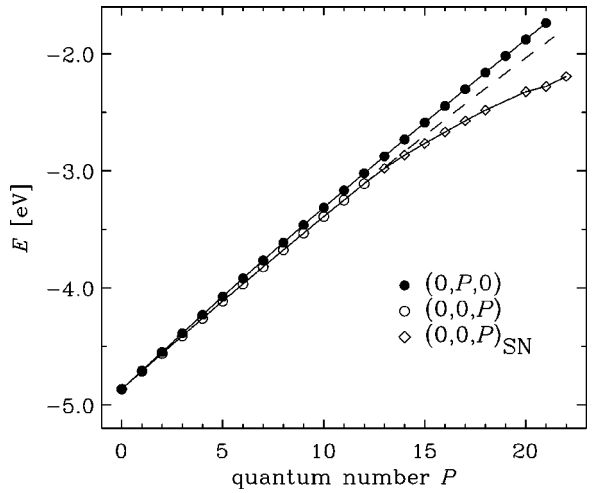

FIG. 11. Energies of levels $(0,P,0)$ and $(0,0,P)$ vs polyad quantum number P. Starting with $P=13$ the energies of the [SN] states are shown. The dashed curve is an extrapolation of the data points with $P\leqslant 12$.

and $(0,0,P)$; according to the discussion above, the $(0,0,P>12)$ states are really $(0,0,P)_{SN}$ states. The $(0,P,0)$ progression shows a rather small anharmonicity up to very high levels. This is in line with the observation that the period of the corresponding $[B]$ PO does not change much with energy. The other progression, $(0,0,P)$, is slightly more anharmonic with the result that the gap between the two ladders slowly increases. It exists only up to $P=12$, where the $(0,0,P)_{SN}$ progression abruptly sets in. The latter is highly anharmonic, which explains why the corresponding levels do not fit well into the general polyad structure but appear at significantly lower energies than expected. The [SN]-type wave functions have a completely different structure than the $[r1A]$-type wave functions and extend more towards the isomerization path. Since the potential becomes gradually flatter along the minimum energy path, it is not surprising to observe a significant reduction in the energy spacing and therefore an increase of the anharmonicity (see Fig. 2).

The dashed line in Fig. 11 is an extrapolation of the $[r1A]$ progression derived from a fit to the energies up to level (0,0,12). It appears that the structural change of the wave functions begins just where the $(0,0,P)$ and the $(0,0,P)_{SN}$ curves ''bifurcate.'' Expressed differently, while climbing up the ladder, the quantum mechanical wave functions follow the [SN]-type path rather than the $[r1A]$ route at the bifurcation.

The structural change of the states is also encoded in the energy spacing between adjacent levels, $\Delta E_P(n)=E_{(0,P-n,n)}-E_{(0,P-n-1,n+1)}$, within a particular polyad. For the lower polyads $\Delta E_P(n)$ monotonically increases from the lowest to the highest level as can be seen in Fig. 12, i.e., the spacing is smallest at the bottom of a polyad and largest at the top. This monotonic behavior holds true up to $P=9$ and 10. Starting with $P=11$, $\Delta E_P(n)$ becomes nonmonotonic having a minimum at $n=9$. This minimum shifts to $n=11$ for $P=13$ and then stays at 11. The two different branches for the higher polyads indicate the change from the $[r1A]$- to the $[B]$-type behavior at the lower end of a polyad. Whether this minimum in the energy spacing has the same origin as the one predicted in the effective Hamiltonian analysis of Kellman and co-workers,[53] has to be investigated in the future.

Up to now we exclusively analyzed levels without excitation in the third coordinate, R. The general behavior discussed for the $v_1=0$ states does not qualitatively change when $v_1\neq 0$. Around the same energy, where the $(0,v_2,v_3)$ states show a transition from the $[r1A]$-type wave functions to the [SN] wave functions, the wave functions for states with excitation in R show a similar change. Examples for two polyads, $(1,P=12)$ and $(2,P=10)$, are depicted in Fig. 13. However, in comparison with the $v_1=0$ states the transition occurs more gradually and not so abrupt. Thus, although the polyad structure and the change of the structure of the molecule is not strongly dependent on R, the motions in r and γ, on one hand, and in R, on the other, are not completely decoupled. The distinctly different level spacings within polyads for different quantum numbers v_1 further support this conjecture (see Figs. 6 and 9).[56]

Despite the fact that substantial mixing of all three

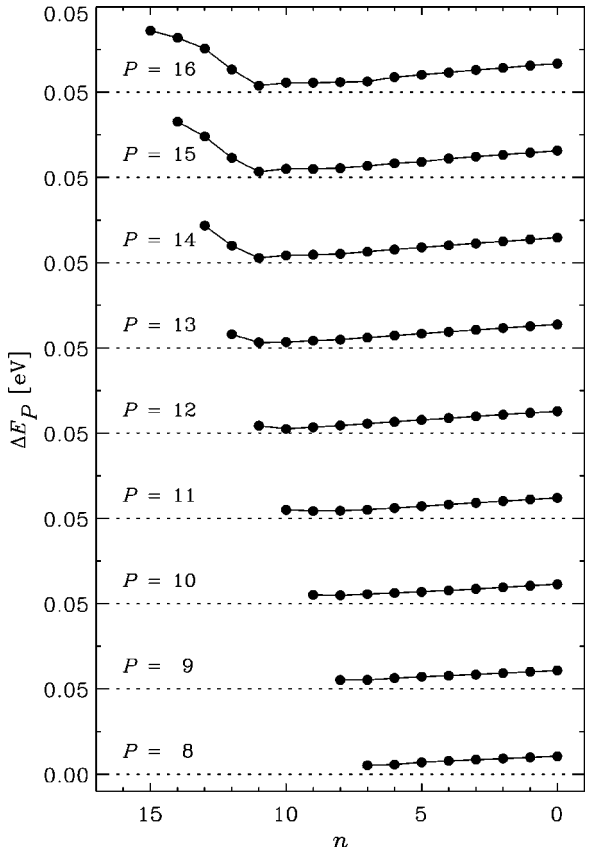

FIG. 12. Energy spacing between adjacent levels within a particular polyad, $\Delta E_P(n)$, as function of $n\geqslant 0$. $n=0$ marks the top of the polyad. (See text for further details.)

modes gradually prohibits the complete assignment of states for higher and higher energies, it is possible to assign all of the $[B]$-type and most of the [SN]-type overtones. In Table IV we list the energies and the energy differences, ΔE, between adjacent levels of the $(0,v_2,0)$ and the $(0,0,v_3)_{SN}$ states. Examples of higher-order SN-type wave functions are depicted in Fig. 14. It is clearly seen how the [SN]-type wave functions penetrate deeper and deeper into the CP–H hemisphere of the PES as the energy increases. For comparison we show one [SN] PO in the upper two panels together with a contour plot of the potential. Because at these high energies several families of [SN] orbits coexist, it is not clear which type corresponds to a particular wave function. For the $(0,v_2,0)$ states ΔE decreases in a very regular manner with increasing quantum number, which indicates that this progression is very robust and is not significantly perturbed by coupling to other modes. In contrast, ΔE for the SN states has a less gradual dependence. In view of the energy spacings there seem to be at least two different families of SN-type states; a third one might begin with the highest overtone considered, which we reluctantly assigned to $((0,0,26))_{SN}$ (unclear assignments are put in double brackets). Since the states $(0,0,14)_{SN}$, $(0,0,19)_{SN}$, and $(0,0,25)_{SN}$ are missing in the table (because of substantial mixing with other states, the wave functions do not have a clear nodal structure), the overall picture is somehow blurred. Although a direct correlation

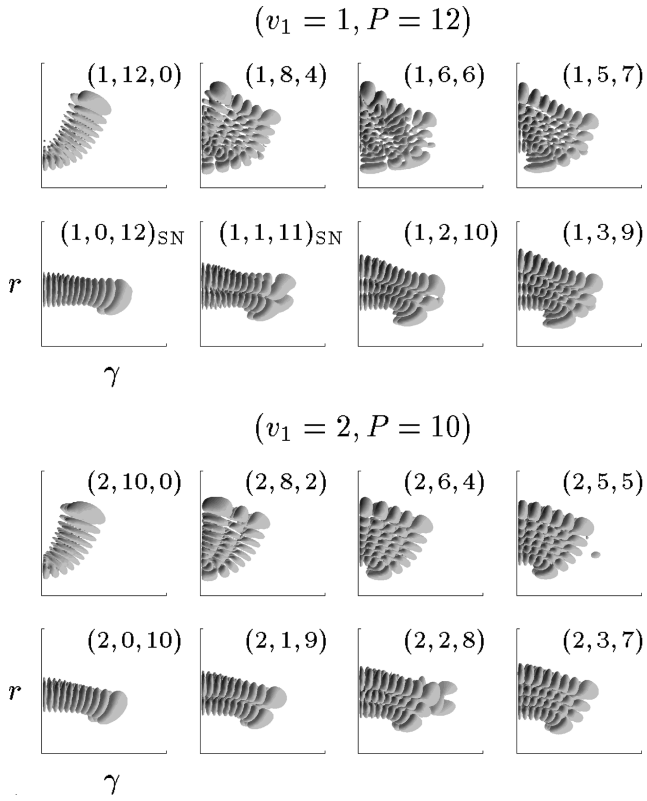

FIG. 13. Wave functions for polyads $(1,P=12)$ and $(2,P=10)$. For further details see Fig. 7.

TABLE IV. Assigned overtone states of the $[B]$ and the [SN] type.

$[B]$ state	E/cm^{-1}	$\Delta E/\mathrm{cm}^{-1}$	[SN] State	E/cm^{-1}	$\Delta E/\mathrm{cm}^{-1}$
(0,0,0)	0				
(0,1,0)	1 283	1283			
(0,2,0)	2 568	1285			
(0,3,0)	3 850	1282			
(0,4,0)	5 124	1274			
(0,5,0)	6 388	1264			
(0,6,0)	7 639	1251			
(0,7,0)	8 877	1238			
(0,8,0)	10 101	1224			
(0,9,0)	11 311	1210			
(0,10,0)	12 509	1198			
(0,11,0)	13 697	1188			
(0,12,0)	14 875	1178	(0,13,0)	15 211	
(0,13,0)	16 045	1170	(0,15,0)	16 931	*1720*[a]
(0,14,0)	17 208	1163	(0,16,0)	17 713	782
(0,15,0)	18 366	1158	(0,17,0)	18 482	769
(0,16,0)	19 519	1153	(0,18,0)	19 221	739
(0,17,0)	20 668	1149	(0,20,0)	20 493	*1272*
(0,18,0)	21 813	1145	(0,21,0)	20 862	369
(0,19,0)	22 955	1142	(0,22,0)	21 228	366
(0,20,0)	24 097	1142	(0,23,0)	21 548	320
(0,21,0)	25 235	1138	(0,24,0)	21 825	277
			((0,26,0))	22 721	*896*

[a]The italic numbers do not correspond to nearest neighbors spacings.

of wave functions and POs of the different [SN]-type or energy spacings and classical periods is difficult, the rather abrupt change of the energy spacing in the saddle-node states indicates that the quantum mechanical states are indeed influenced by the different [SN]-type classical orbits.

V. ROTATIONAL CONSTANTS

In a spectroscopic experiment one measures energy differences rather than wave functions. Information about the structure of a particular vibrational state can be extracted only indirectly from intensities or, more precisely, from fine structure constants such as, for example, rotational constants. In the case of HCP, the two quite different bending motions, represented by the $[B]$- and the $[r1A]$-type wave functions, on one hand, and wave functions with [SN] character, on the other, result in substantially different rotational constants and therefore rotational constants are helpful quantities for identifying different structures of vibrational states.[30]

In the present work we determined the rotational constants for each of the 700 vibrational levels by calculating the expectation values of the inverse of the moments of inertia with the $J=0$ eigenfunctions. The moments of inertia have been calculated by diagonalizing the inertia tensor. Of course, this procedure for calculating rotational constants is an approximation and effects due to modifications of the vibrational wave functions as a consequence of overall rotation and Coriolis coupling are not taken into account. The rotational constant for rotation around an axis in the HCP plane and approximately perpendicular to the CP axis, B_{rot}, is close to the spectroscopic B_0 measured by Ishikawa *et al.*[24]

In general, the B_{rot} values for the states with wave functions of the [SN]-type are substantially larger than those for the $[B]$- and $[r1A]$-type states. The differences can be qualitatively explained in terms of the quite different amplitudes of bending motion for the three families of states. The main contribution to the moment of inertia results from rotation of CP around the axis, while the contribution from the much lighter H atom is exceedingly smaller. However, in the case of the small-amplitude angular motion of the $[B]/[r1A]$ states, the hydrogen atom is always far away from the rotation axis with the result that its contribution is not negligible, but of the order of at least a few percent of the contribution of the CP rotation. On the other hand, in the case of the large-amplitude angular motion of the [SN] states the H atom spends most of the time close to the rotation axis ($\gamma \approx 90°$) so that its net contribution is indeed unimportant. Since the rotational constant is proportional to the inverse of the moment of inertia, the $[B]/[r1A]$ states have a rotational constant which is a few percent smaller than for the [SN] states.

First, we consider the variation of B_{rot} inside a particular polyad. In Fig. 15(a) we plot B_{rot} for states $(0,P-n,n)$ with $n=0$ (the highest member of the polyad) through $n=P$ (the lowest member of the polyad). For small values of P, the rotational constant monotonically decreases with n from the top to the bottom of the polyad, with the exception of the lowest level. This general behavior can be qualitatively explained by the more or less monotonic decrease of the expectation value $\langle\gamma\rangle$ from state $(0,P,0)$ to $(0,0,P)$ (see for

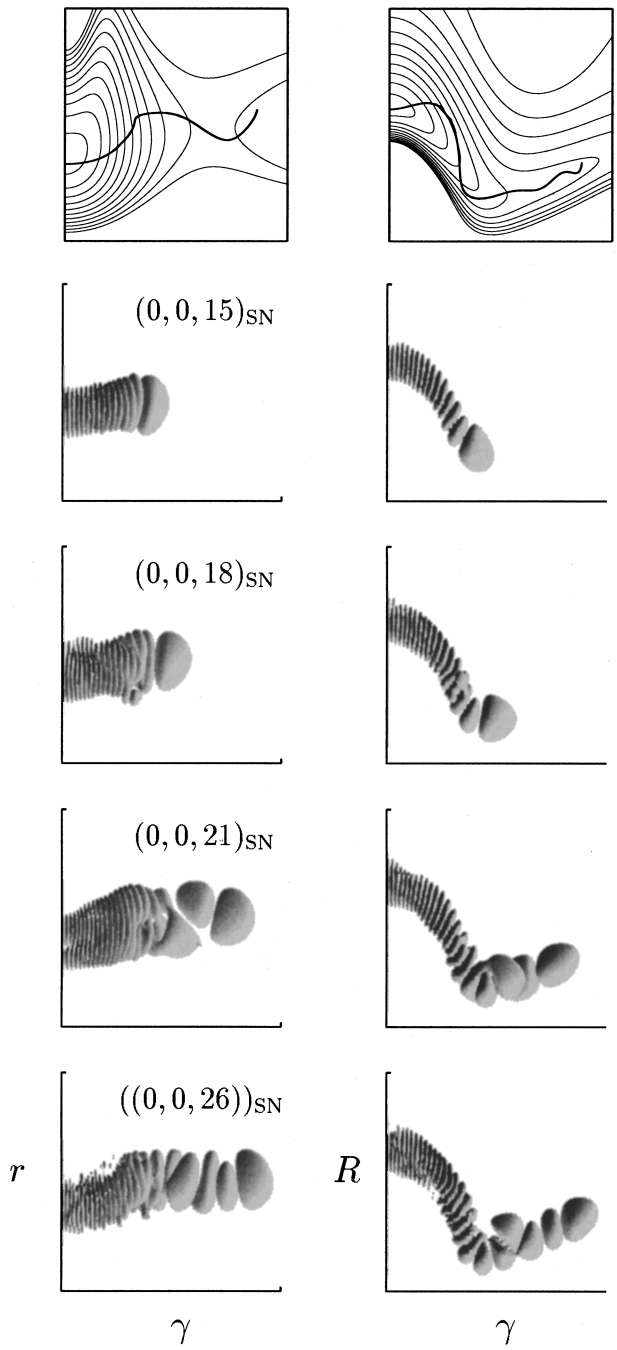

FIG. 14. Examples of wave functions for higher overtones of [SN]-type states. The horizontal axis ranges from $\gamma=0$ to 140° and the vertical axes range from $r=2.32\ a_0$ to $r=4.00\ a_0$ and from $R=1.58\ a_0$ to $R=6.00\ a_0$, respectively. The appropriate cuts through the PES are depicted in the upper panels together with a periodic orbit of [SN] type for $E=-2.25$ eV. For more details see Ref. 52.

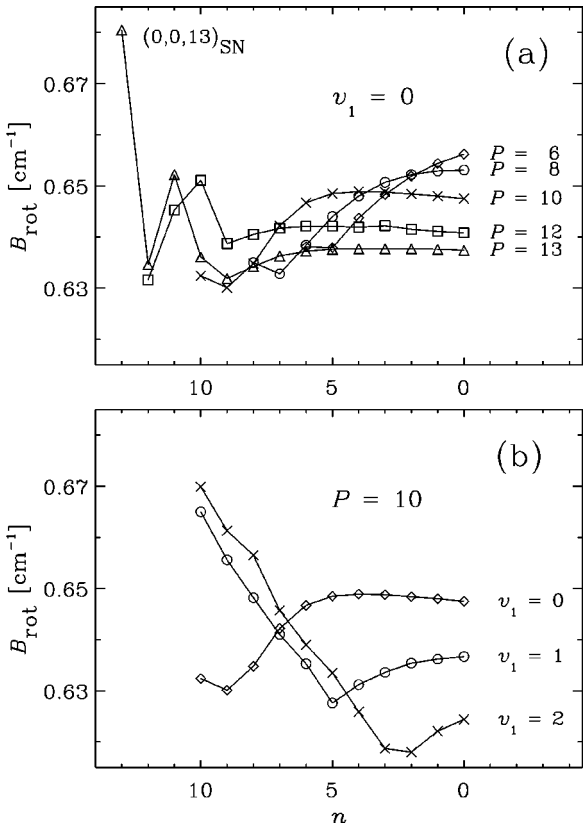

FIG. 15. (a) Rotational constants B_{rot} for states $(0,P-n,n)$ as function of n for several polyads. $n=0$ marks the top of the polyads. (b) The same as in (a) but for states $(v_1\leqslant 2,\ P-n,n)$ with $P=10$.

example polyad $P=3$ in Fig. 7). The smaller $\langle\gamma\rangle$ the larger is the distance of H from the rotation axis and, as a consequence, the smaller is the rotational constant. With increasing polyad quantum number the behavior changes slightly in that B_{rot} first stays approximately constant before it decreases near the lower end of the polyad.

The overall picture changes quite substantially with $P=12$ where the perturbations of the wave functions in the low-energy portion of the polyad become more distinct. The rotational constants for states (0,2,10) and (0,1,11) are much larger than they are expected to be. The corresponding wave functions shown in Fig. 8 have some clear admixture of SN character, which explains this increase of B_{rot}. State (0,0,12) is again a ''normal'' $[r1A]$ state and its rotational constant is again much smaller than for the next two higher levels. The first real [SN]-type state occurs in the $P=13$ polyad and for reasons discussed above the corresponding rotational constant is significantly larger than the constants for all lower states. Figure 15(b) shows, for $P=10$, similar results for states with excitation in the ν_1 mode. With increasing excitation in the H–CP stretching mode the transition from $[B]$- or $[r1A]$-type behavior to [SN]-type behavior occurs at higher and higher members in the polyad (smaller values of n) and the rotational constants clearly show this. In conclusion, the rotational constant reflects in a remarkable manner the structure of the vibrational states, especially the extent of the angular motion.

In Fig. 16(a) we plot the rotational constants for the 700 lowest states as a function of energy. One can clearly distinguish two regimes: States whose B_{rot} constants are below the rotational constants belonging to the $(0,P,0)$ progression and states above this borderline. The $(0,P,0)$ states can be uniquely identified up to very high energies and their rotational constants vary exceedingly smoothly with P [Fig. 16(b)]. In accord with experiment[24] they first rise with en-

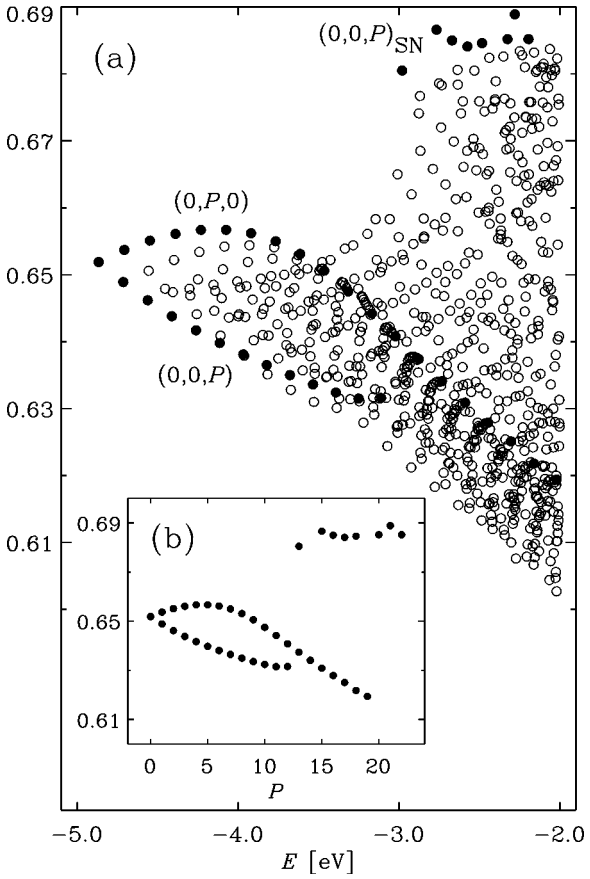

FIG. 16. (a) Rotational constants B_{rot} for the lowest 700 states as function of energy. The constants for the three overtone progressions $(0,P,0)$, $(0,0,P)$, and $(0,0,P)_{SN}$ are indicated by solid dots and drawn separately in (b).

ergy and then monotonically decrease with P. The B_{rot} values for progression $(0,0,P)$ monotonically decrease with P up to $P=12$. In accord with our calculations, the measured value for (0,0,1) is slightly lower than the rotational constant for the vibrational ground state (Table VIII in Ref. 36). As discussed in Sec. IV the $(0,0,P)$ progression only extends to $P=12$. State (0,0,13) is of the [SN] type and because of the essentially different angular shape, this state has a much larger rotational constant. States (0,0,14) and (0,0,19) are strongly perturbed and therefore not included in the progression. The many states between the $(0,P,0)$ progression on one hand and the $(0,0,P)_{SN}$ progression on the other have more or less pronounced [SN] character and therefore rotational constants which are larger than those for the pure $[B]$-type states.

Except for the lower states of the $(0,P,0)$ progression, the rotational constants for states $(0,P,0)$ and $(0,0,P)$ decrease with energy. This behavior can be explained by the continuous increase of the expectation value of the CP stretching coordinate, $\langle r\rangle$, with the degree of excitation. On the other hand, $\langle r\rangle$ remains approximately constant with P for the [SN] states and so does the corresponding B value.

VI. DISCUSSION

Demonstrating how the vibrational energy spectrum of HCP, a relatively simple triatomic molecule, changes with energy and how new types of motions appear when climbing up the ladder were the main purposes of the foregoing sections. Classical mechanics, especially the concept of periodic orbits and their continuation/bifurcation diagram, have been proven to be exceedingly helpful in understanding the development of the quantum mechanical states. Nevertheless, if one wants to obtain a clearest picture, it is absolutely necessary to visually inspect all wave functions, even though that is a tremendous task. Automatic assignments in terms of, for example, projections of wave functions on zero-order wave functions, works at low energies, but is bound to fail when mixing of (zero-order) states becomes too strong.

The most surprising finding was the gradual change of the polyad structure at the bottom of the polyad, when the states $(0,0,P)$ with wave functions quite restricted in the H–C–P bending angle turn into $(0,0,P)_{SN}$ states, whose wave functions have a completely different bending behavior. Although this transition sets in rather abruptly in a narrow energy regime, early signs of these structural changes are already found at lower energies. The onset of this change is accurately predicted by classical mechanics in form of the birth of saddle-node periodic orbits. In contrast to classical mechanics where the [SN]-type POs come into existence at a precise energy, in quantum mechanics the structural change is, as expected, somehow smeared out. It should be noted that the $[r1A]$-type wave functions do not completely cease to exist. At higher energies one can find wave functions that have, if the contours plotted are chosen in a special way, the character of $(0,0,P)$ wave functions. However, the examples found by us were strongly mixed with other states in the energetic proximity. In other words, quantum mechanics still ''feels'' the existence of the underlying $[r1A]$ POs.

There are several interesting questions to be asked and classical mechanics can provide possible answers to them. First, why does the change begin at the bottom of the polyads and not at the top, i.e., why do the $(0,0,P)$ states turn into the saddle-node wave functions rather than the $(0,P,0)$ levels? We think the answer to this question has to do with the different stabilities of the $[B]$- and $[r1A]$-type POs. The $[B]$ periodic orbits and likewise the corresponding wave functions are comparably robust and exist up to very high energies; in addition the anharmonicity is quite small in this mode. One reason for this pronounced stability might be the existence of the potential trough seen at small angles and larger CP bond distances (Fig. 1), which—loosely speaking—''guides'' the $[B]$ orbits. The sibling POs of the $[r1A]$-type avoid this region of the PES and intuitively are expected to be less stable. Actually, they eventually cease to exist at around -2 eV, an energy where the $[B]$ orbits are still intact. Moreover, the classical bifurcation analysis showed that there is a second branch of trajectories, $[r1B]$, which are unstable and therefore create regions of instability in their neighborhood. Thus, it appears that first the quantum mechanical states, which follow the less stable POs, change their character.

Second, why do the SN POs and the corresponding quantum states come into existence so suddenly with energy? According to general results of non-linear dynamics

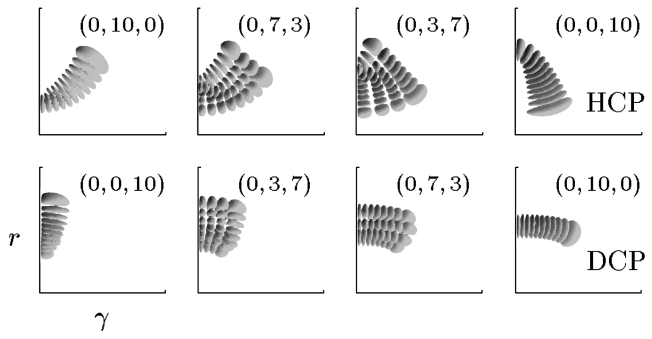

FIG. 17. Comparison of selected HCP and DCP wave functions in polyad $P=10$. For more details see Fig. 7.

theories, saddle-node bifurcations occur as a consequence of tangencies of the stable and unstable manifolds of unstable periodic orbits. As predicted by the Newhouse theorem,[57] when these invariant objects (the manifolds) touch each other, new periodic orbits emerge. By way of this mechanism classical trajectories find ways to penetrate into regions of phase space, which were not sampled by periodic orbits at lower energy. Characteristic examples are the saddle-node bifurcations which appear above potential barriers. The unstable POs that originate at the top of the barrier give rise to periodic orbits which can visit the minima on both sides of the barrier.[19,22,58] The remarkable observation is that these saddle-node POs create stability in otherwise highly unstable regions of phase space. Studies like the present one demonstrate how quantum mechanics can ''recognize'' these regions and accommodates the eigenfunctions accordingly.

Saddle-node bifurcations may also appear inside potential wells when the curvature of the potential changes abruptly.[59,60] This is the case for HCP. As we can see from Fig. 2 the saddle-node bifurcations emerge when the minimum energy path signals changes in the slope of the PES. It is really astonishing that the quantum mechanical states of the SN type appear at about the same energies and show distinct progressions with different energy spacings. This underlines the strong influence the different [SN]-type POs have on the quantum mechanical world.

The third question concerns the relative importance of kinetic energy coupling and coupling of the modes due to the potential. In the initial phase of our study we believed that it is the pronounced potential trough mentioned above that explains the bowed shape of the $[B]$-type POs and the corresponding wave functions. However, if that were true, how can we explain—in terms of the shape of the PES—the particular form of the $[r1A]$ POs and wave functions? In doing the mass variation study discussed in Sec. IV we found out that the interplay between the kinetic energy term and the potential is important. In Fig. 17 we show wave functions for HCP in polyad $P=10$ in comparison to the corresponding wave functions for DCP. Although there is some mixing between r and γ, the wave functions for DCP have a much stronger local-mode character, i.e., they are much better aligned along the r and the γ axis. The $(0,P,0)$ bending states extend along the isomerization path and this behavior is not just found at high energies but even for the lowest excited states. A detailed discussion of DCP will be published at a later date.

The accuracy of our PES is not sufficient to compare directly the calculated transition energies and rotational constants with the experimental results. For example, the discrepancy for the fundamental of the $(0,P,0)$ progression is $53\ \mathrm{cm}^{-1}$, which accumulates up to about $300\ \mathrm{cm}^{-1}$ for the 14th overtone. Beyond $P=15$ the deviation becomes smaller again. This large mismatch and the relatively large density of states makes it impossible to uniquely relate the measured transitions to the vibrational levels calculated. Therefore, we are unable to identify the calculated levels that correspond to the levels for which unusually large rotational constants have been measured. At present time the comparison can only be made qualitatively.

It is plausible to speculate that the onset of the perturbations detected in the $(0,v_2,0)$ progression[24] with $v_2 \geqslant 16$ (in our notation) is caused by the structural changes of the quantal wave functions found in the present study. Between $v_2=17$ and 19 the measured B_{rot} value changes substantially by about 8% and takes on values which are in very good agreement with the calculated rotational constants for the SN states. Although this agreement might be coincidence, we have the impression that the sudden increase signals some structural changes of the kind described by us. In an attempt to assess the existence of the [SN]-type states, Ishikawa *et al.*[31] performed an additional SEP experiment and indeed found bands having the characteristics of the $(0,0,P)_{\mathrm{SN}}$ states; relatively large rotational constants, a large anharmonicity, and an energetic origin in reasonable agreement with our predictions.

What is needed is a better potential energy surface in order to directly compare with the experimental spectra. At present time the *ab initio* calculations of Koput[38] are extended to cover the full angular regime from H–CP to CP–H. Once this PES is available we should be in the position to make a rigorous contact with experiment.

Recently there has been some interest in extracting information about periodic orbits and their bifurcations from quantum mechanical spectra alone, without actually searching for POs.[61,62] The tool is a windowed Fourier transformation of the quantum mechanical spectrum (called vibrogram[61]), i.e.,

$$A(T,E)=\int_{-\infty}^{+\infty}\Sigma(\epsilon)f(E-\epsilon)e^{-i\epsilon T}d\epsilon, \tag{6}$$

where the spectrum $\Sigma(\epsilon)$ is given by

$$\Sigma(\epsilon)=\sum_n \delta(\epsilon-\epsilon_n), \tag{7}$$

and the sliding window $f(\epsilon)$ is a Gaussian. The results, which we obtained when taking the calculated vibrational energies without any weighting, were not satisfactory. Especially the sudden occurrence of the saddle-node POs could not be seen. A clearer picture emerged, however, when absorption-type spectra, calculated with localized initial-state

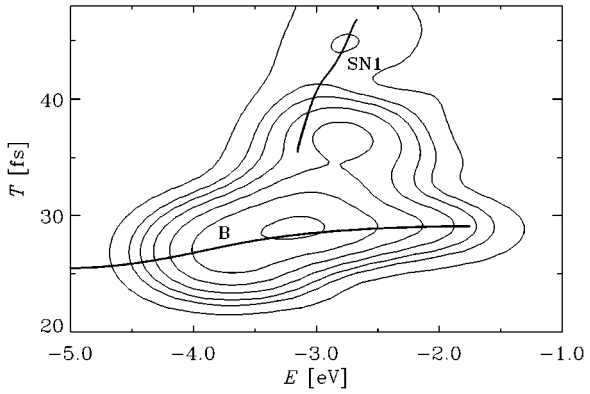

FIG. 18. Vibrogram $|A(T,E)|^2$ obtained from quantum mechanical absorption-type spectra as described in the text. The solid lines are the energy-dependent half-periods of the $[B]$- and $[\mathrm{SN1}A]$-type periodic classical orbits.

wave functions, were Fourier transformed. Thus, in order to see, for example, the $[B]$ POs we put Gaussian wave functions on the corresponding orbits, calculated the overlap with all vibrational states and used this spectrum in Eq. (6). The same was done with wave packets localized on the [SN] periodic orbits. Various vibrograms were compiled into a total vibrogram with the interference between different wave packets taken into account. An example is shown in Fig. 18. One clearly sees the bifurcation around -3 eV. For comparison, we also depict the half-periods of the $[B]$ and $[\mathrm{SN1}A]$ periodic orbits and good overall agreement is observed. (Because in the classical calculations the angular coordinate is allowed to vary between $-180°$ and $+180°$, it is $T/2$ that corresponds to $2\pi/\Delta E$, where ΔE is the energy spacing between two levels.) Thus, information about the time-energy relationship of classical periodic orbits can be obtained from only the quantum mechanical calculations, provided the ''spectra'' are prepared in a particular manner. This requires, however, that some knowledge about the POs is already available.

VII. CONCLUSIONS

Our classical and quantum mechanical calculations for the energy spectrum of HCP in the ground electronic state, using an *ab initio* PES, have revealed the following clues:

(1) The spectrum is governed by a 1:1 (1:2, if conventional spectroscopic nomenclature is used) resonance between CP stretching and H–C–P bending motion leading to a substantial mixing of local-mode states. The spectrum, which consists of clearly defined polyads, as well as the normal-mode wave functions are astonishingly regular, even at energies where anharmonic couplings due to the potential are prominent.
(2) All states below some critical energy are confined to the H–CP hemisphere, i.e., the (Jacobi) angle γ remains smaller than 40° or so, even if the energy is sufficiently high for following the isomerization path to CP–H.
(3) A new class of states, which follows the isomerization path all the way to the CP–H side with increasing energy, suddenly comes into existence at a relatively high energy. At the same time the polyad structure gradually disintegrates with the wave functions at the bottom of the polyad turning into the isomerization bending states.
(4) Classical periodic orbits quantitatively describe all the findings observed in the quantum calculations. In particular, they closely follow the backbone of the quantal wave functions and explain the sudden appearance of the isomerization-type bending states as the consequence of a saddle-node bifurcation. They even predict the abrupt change of energy spacing between neighboring saddle-node overtones through the generation of new saddle-node periodic orbits at higher energies.
(5) The two classes of bending states, those which are confined in the angular coordinate and those which follow the isomerization path, have distinctly different moments of inertia reflecting the small- and large-amplitude bending motions. The resulting rotational constants for rotation about an axis perpendicular to the CP axis agree well with the two regimes observed in recent SEP spectroscopy experiments.
(6) Although a direct comparison with experimental data is, because of the limited accuracy of the potential energy surface used, not possible, our calculations qualitatively explain several observations such as the abrupt onset of perturbations observed in the experimental SEP spectra, the existence of states with two classes of rotational constants, as well as the reality of states with unusually large anharmonicity.

ACKNOWLEDGMENTS

S.C.F. and R.S. are very grateful to R. W. Professor Field for stimulating their interest in the spectroscopy of HCP and, most importantly, for many invaluable discussions. We also thank H. Ishikawa for sending a copy of Ref. 31 prior to publication. S.C.F. acknowledges financial support through the Sonderforschungsbereich 357 ''Molekulare Mechanismen Unimolekularer Reaktionen'' and the Max-Planck-Institut für Strömungsforschung during his stay at Göttingen where part of this work was carried out. C. B. and R. S. also acknowledge financial support by the DFG through the Sonderforschungsbereich 357. S.Yu.G. thanks the Alexander von Humboldt Stiftung for financial support.

[1] *Molecular Dynamics and Spectroscopy by Stimulated Emission Pumping*, edited by H.-L. Dai and R. W. Field (World Scientific, Singapore, 1995).
[2] R. E. Wyatt, in *Lasers, Molecules, and Methods*, edited by J. R. E. Wyatt and R. D. Coalson (Wiley, New York 1989), p. 231.
[3] R. Kosloff, Annu. Rev. Phys. Chem. **45**, 145 (1994).
[4] H.-J. Werner, C. Bauer, P. Rosmus, H.-M. Keller, M. Stumpf, and R. Schinke, J. Chem. Phys. **102**, 3593 (1995).
[5] H.-M. Keller, H. Floethmann, A. J. Dobbyn, R. Schinke, H.-J. Werner, C. Bauer, and P. Rosmus, J. Chem. Phys. **105**, 4983 (1996).
[6] H.-M. Keller, T. Schröder, M. Stumpf, C. Stöck, F. Temps, R. Schinke, H.-J. Werner, C. Bauer, and P. Rosmus, J. Chem. Phys. **106**, 5333 (1997).
[7] M. J. Davis, J. Chem. Phys. **98**, 2614 (1993).
[8] M. J. Davis, Int. Rev. Phys. Chem. **14**, 15 (1995).
[9] S. L. Coy, D. Chasman, and R. W. Field, in *Molecular Dynamics and Spectroscopy by Stimulated Emission Pumping*, edited by H.-L. Dai and R. W. Field (World Scientific, Singapore, 1995), p. 891.

[10] E. J. Heller, in *Chaos and Quantum Physics*, edited by M. Giannoni, A. Voros, and J. Zinn-Justin (Elsevier, Amsterdam, 1991).
[11] M. C. Gutzwiller, J. Math. Phys. **8**, 1979 (1967).
[12] M. C. Gutzwiller, J. Math. Phys. **12**, 343 (1971).
[13] M. C. Gutzwiller, *Chaos in Classical and Quantum Mechanics* (Springer, Bellin, 1990), Vol. 1.
[14] E. J. Heller, Phys. Rev. Lett. **53**, 1515 (1984).
[15] P. O'Connor, J. Gehlen, and E. J. Heller, Phys. Rev. Lett. **58**, 1296 (1987).
[16] J. M. G. Llorente and E. Pollak, Annu. Rev. Phys. Chem. **43**, 91 (1992).
[17] H. S. Taylor, in *Molecular Dynamics and Spectroscopy by Stimulated Emission Pumping*, edited by H.-L. Dai and R. W. Field (World Scientific, Singapore, 1995), p. 891.
[18] R. Schinke, *Photodissociation Dynamics* (Cambridge University Press, Cambridge, 1993).
[19] S. C. Farantos, Int. Rev. Phys. Chem. **15**, 345 (1996).
[20] E. L. Allgower and K. Georg, *Numerical Continuation Methods*, Vol. 13 in Springer Series in Computational Mathematics (Springer, Bellin, 1993).
[21] R. Prosmiti and S. C. Farantos, J. Chem. Phys. **103**, 3299 (1995).
[22] S. C. Farantos, Laser Chem. **13**, 87 (1993).
[23] G. Contopoulos, S. C. Farantos, H. Papadaki, and C. Polymilis, Phys. Rev. E **50**, 4399 (1994).
[24] H. Ishikawa, Y.-T. Chen, Y. Ohshima, B. Rajaram, J. Wang, and R. W. Field, J. Chem. Phys. **105**, 7383 (1996).
[25] K. K. Lehmann, S. C. Ross, and L. L. Lohr, J. Chem. Phys. **82**, 4460 (1985).
[26] Y.-T. Chen, D. M. Watt, R. W. Field, and K. K. Lehmann, J. Chem. Phys. **93**, 2149 (1990).
[27] M. A. Mason and K. K. Lehmann, J. Chem. Phys. **98**, 5184 (1993).
[28] J. W. C. Johns, H. F. Shurvell, and J. K. Tyler, Can. J. Phys. **47**, 893 (1969).
[29] A. Cabaña, Y. Doucet, J.-M. Garneau, C. Pépin, and P. Puget, J. Mol. Spectrosc. **96**, 342 (1982).
[30] S. C. Farantos, H.-M. Keller, R. Schinke, K. Yamashita, and K. Morokuma, J. Chem. Phys. **104**, 10 055 (1996).
[31] H. Ishikawa, C. Nagao, N. Mikami, and R. W. Field, J. Chem. Phys. **106**, 2980 (1997).
[32] MOLPRO is a package of *ab initio* programs written by H.-J. Werner and P. J. Knowles, with contributions from J. Almlöf, R. D. Amos, M. J. O. Deegan, S. T. Elbert, C. Hampel, W. Meyer, K. Peterson, R. Pitzer, A. J. Stone, and P. R. Taylor.
[33] J. N. Murrell, S. Carter, S. C. Farantos, P. Huxley, and A. J. C. Varandas, *Molecular Potential Energy Functions* (Wiley, New York, 1984).
[34] J. N. Murrell, S. Carter, and L. O. Halonen, J. Mol. Spectrosc. **93**, 307 (1982).
[35] X. Liu and J. N. Murrell, J. Chem. Soc. Faraday Trans. **88**, 1503 (1992).
[36] M. Jung, B. P. Winnewisser, and M. Winnewisser (submitted).
[37] C. Puzzarini, R. Tarroni, P. Palmieri, J. Demaison, and M. L. Senent, J. Chem. Phys. **105**, 3132 (1996).
[38] J. Koput, Chem. Phys. Lett. **263**, 401 (1996).
[39] J. Koput and S. Carter, Spectrochim. Acta A **53**, 1091 (1997).
[40] S. C. Farantos, J. Mol. Struct.: THEOCHEM **341**, 91 (1995).
[41] A. Weinstein, Invent. Math. **20**, 47 (1973).
[42] J. Moser, Commun. Pure Appl. Math. **29**, 727 (1976).
[43] J. Guckenheimer and P. Holmes, *Nonlinear Oscillations, Dynamical Systems, and Bifurcations of Vector Fields* (Springer, Berlin, 1983).
[44] R. Seydel, *From Equilibrium to Chaos: Practical Bifurcation and Stability Analysis* (Elsevier, New York, 1988).
[45] E. Reithmeier, *Periodic Solutions of Nonlinear Dynamical Systems*, Lecture Notes in Mathematics (Springer, Berlin, 1991).
[46] Of course, a periodic orbit does not have an initial point in the phase space. With initial point we mean here that particular point at which the tracing of the periodic orbit from E to $E+\delta E$ is started. A more rigorous procedure would be to choose, for example, the maximum value of r along the PO for a particular energy. That would change the various curves in the bifurcation diagram but not the general appearance nor the bifurcation points.
[47] More information about the calculated periodic orbits can be found at the www site http://www.cc.forth.gr/farantos/articles/hcp/data/
[48] A. J. Dobbyn, M. Stumpf, H. Keller, and R. Schinke, J. Chem. Phys. **103**, 9947 (1995).
[49] The accuracy of the quantum calculations can be approximately assessed by comparing the number of quantum mechanical states at a particular energy with the corresponding number extracted from the volume of the classical phase space. For the energy of the 250th state, E_{250}, the phase-space volume gives 253. For E_{500}, E_{750}, and E_{1000} the corresponding classical numbers are 506, 755, and 1004, respectively. Because of the polyad structure the quantum mechanical number of states $N(E)$ is not a smooth function of E, which partly explains the relatively large deviations for the smaller energies. Overall, however, the agreement is very good.
[50] The results of the quantum mechanical calculation together with the assignment can be obtained by anonymous ftp from ftp.gwdg.de, directory/ftp/public/mpsf/schinke/hcp/quantum.results.
[51] H. D. Mordaunt, H. Flöthmann, M. Stumpf, H.-M. Keller, C. Beck, R. Schinke, and K. Yamashita, J. Chem. Phys. **107**, 6603 (1997).
[52] All the wave function plots shown in this article have been obtained from a 3D plotting routine, which allows to rotate objects, that depend on three variables, in space. In all cases we show one particular contour $\epsilon(R,r,\gamma)=\sin\gamma|\Psi(R,r,\gamma)|^2$ with the value of ϵ being the same within one figure. The plots are always viewed along the R axis, i.e., in the direction perpendicular to the (r,γ)-plane. Especially the wave functions of highly excited states (or their backbones) are not confined to the (r,γ)-plane but arranged in the 3D space. Therefore, showing 2D projections, with one coordinate fixed or integrated over, makes their appearance less informative. The shading emphasizes the 3D character of the wave functions. After testing various ways of plotting we came to the conclusion that these representations are optimal.
[53] M. E. Kellman, in *Molecular Dynamics and Spectroscopy by Stimulated Emission Pumping*, edited by H.-L. Dai and R. W. Field (World Scientific, Singapore, 1995).
[54] M. E. Kellman, Annu. Rev. Phys. Chem. **46**, 395 (1995).
[55] In paper I the $(0,0,P)_{\mathrm{SN}}$ states had been labeled $(0,P,0)_{\mathrm{SN}}$. Because these states substitute the real $[r1A]$-type states $(0,0,P)$, we have changed the nomenclature.
[56] We also performed classical as well as quantum mechanical two-dimensional calculations with R fixed at its equilibrium for $\gamma=0$ and found that the 2D and 3D molecules are remarkably different, which shows that all three modes are coupled.
[57] S. E. Newhouse, Publ. Math. IHES **50**, 101 (1979).
[58] S. C. Farantos, Chem. Phys. **159**, 329 (1992).
[59] R. Prosmiti, S. C. Farantos, R. Guantes, F. Borondo, and R. M. Benito, J. Chem. Phys. **104**, 2921 (1996).
[60] F. Borondo, A. A. Zembekov, and R. M. Benito, J. Chem. Phys. **105**, 5068 (1996).
[61] K. Hirai, E. J. Heller, and P. Gaspard, J. Chem. Phys. **103**, 5970 (1995).
[62] M. Baranger, M. R. Haggerty, B. Lauritzen, D. C. Meredith, and D. Provost, CHAOS **5**, 261 (1995).